Experimental investigation under laser-driven shocks of the dynamic behavior of materials for beam-intercepting devices in particle accelerators

Results in Materials 24 (2024) 100638

Contents lists available at ScienceDirect

Results in Materials

journal homepage: www.sciencedirect.com/journal/results-in-materials

Experimental investigation under laser-driven shocks of the dynamic behavior of materials for beam-intercepting devices in particle accelerators☆

C. Accettura [a], L. Baudin [a], A. Bertarelli [a], C. Brabetz [b], F. Carra [a], A.S. Martynenko [b], A. Morena [c,*], A. Moros [a], L. Peroni [c], M. Scapin [c], P. Neumayer [b], M. Tomut [b,d], L. Wegert [b]

[a] CERN, Esplanade des Particules 1, 1211, Geneva, 23, Switzerland
[b] GSI Helmholtzzentrum, Planckstrasse 1, 64291, Darmstadt, Germany
[c] Politecnico di Torino, Corso Duca degli Abruzzi 24, 10129, Turin, Italy
[d] Institute of Materials Physics, University of Munster, Wilhelm-Klemm Strasse 10, Muenster, 48149, Germany

A B S T R A C T

In the present work the results of an extensive experimental campaign in which laser-shocks were used to assess the mechanical strength of graphitic materials are presented. The aim of the project was to study innovative advanced materials used in high energy particle accelerators for beam intercepting devices (BIDs), such as collimators, absorber blocks and dumps. In this framework, thin targets of graphitic materials relevant for the use as particle accelerator BIDs were submitted to high-power laser driven shocks at the PHELIX laser facility in GSI. Online diagnostics such as shadowgraphy and laser velocimetry were deployed together with post-mortem analysis on collected debris and shocked specimens.

The experimental results were compared with results obtained in literature. In this work the data acquired for the performed shots are presented with a focus on graphite samples. The testing campaign provided large amount of information to cross-check and validate the models implemented for laser-matter interaction, shockwave propagation and spall strength concerning a wide range of materials, all relevant for the use in beam intercepting devices of particle accelerators.

1. Introduction

In modern particle accelerators, such as the CERN Large Hadron Collider (LHC) [1,2], the travelling highly energetic particle beams must be safely arrested by beam intercepting devices (BIDs) in accidental scenarios. The BIDs materials must withstand severe thermomechanical conditions due to the quasi-instantaneous energy deposition while also adapting to accelerator operative requirements of high electrical conductivity, ultrahigh vacuum compatibility, geometrical stability and resistance to radiation damage. Furthermore, the material choice should also meet the constraints related to an affordable and large-scale industrial feasibility. In the past, carbon-based structures made of Carbon-fibre Carbon (CFC) composite and isotropic polycrystalline graphite were used in LHC collimators and other beam intercepting devices, nevertheless the development of new particle accelerators with increasing beam intensity and energy imposes challenging requirements for the design of collimators and the selection of their materials. The upgrade project of the LHC at CERN called High-Luminosity LHC (HL-LHC) [3] foresees an increase of the beam intensity by almost a factor of two, to reach five times the design instantaneous luminosity of the LHC, while the Future Circular Collider (FCC) program aims at an increase of the energy stored in the circulating hadron beams (FCC-hh) by almost a factor of 20 with respect to the LHC, reaching up to 8500 MJ [4]. As a consequence of the escalation of beam energy in particle accelerators, the urge of important upgrades of the collimation system [5] is rising and, in particular, the development and characterization of novel materials able to handle even more severe conditions is now becoming a major concern. In this challenging context, CERN has launched an extensive R&D program to explore new solutions in terms of materials fitting the requirements of HL-LHC collimator absorbers [6] with the aim of exploiting the properties of graphitic materials [7–10] and combine them with some well-known high temperature resistance metals [11–15].

Thus far materials that might be exposed to particle bunch impacts have been tested at the HiRadMat facility at CERN [16], however the energy densities reachable in this facility are only a fraction of FCC expected conditions [11,17]. For this reason, the ARIES Work Package 17 aims at finding ways to test materials with energy densities beyond

☆ Research supported by the Aries project.
* Corresponding author.
E-mail address: alberto.morena@polito.it (A. Morena).

https://doi.org/10.1016/j.rinma.2024.100638
Received 22 March 2024; Received in revised form 4 September 2024; Accepted 12 November 2024
Available online 13 November 2024

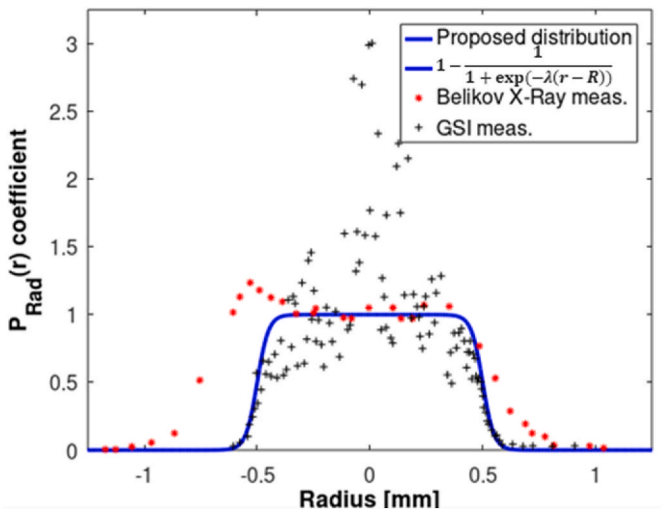

Fig. 1. Spatial distribution of the pressure on the laser beam radius as measured in former works [19,20]. An approximation is proposed for the pressure distribution.

those achievable within the HiRadMat facility and one of the most promising methods is to irradiate with laser shocks. Even though laser and particle beams have differences, they can produce analogous thermo-mechanical effects when they irradiate matter, at least locally. A previous experimental investigation with laser beams was performed on polycrystalline graphite for particle accelerators applications, but only post mortem analysis on the recovered specimens was deployed [18]. Indeed, when interacting with matter both particle and laser pulses induce quasi-instantaneous heating, which can lead to a change of state of the hit surface up to plasma conditions if the energy is high enough. In the framework of the experimental campaign P219 performed at the PHELIX laser facility a wide range of novel materials and coatings relevant for BIDs application were submitted to laser-driven shocks to contribute to their thermo-mechanical characterization under severe loading conditions and estimate the potential damage instantaneously induced on absorber materials in case of accidental hits.

2. Experimental setup

2.1. Presentation

When a high-power laser pulse irradiates a target, it leads to its quasi-instantaneous heating up to plasma condition. Indeed, the plasma expansion, resulting from the laser/matter interaction for nanosecond laser pulses, triggers a compression wave on the front surface of the specimen. The shock wave travels across the target until it reaches the back surface and is reflected as a tensile wave. As a result, a dynamic tensile stress condition is generated below the back surface, which can lead to fragmentation. By changing the intensity of the laser irradiation or the thickness of the specimens, a large range of tensile stresses can be investigated. If this stress reaches the spall strength of the material, the material breaks and a spall can be ejected. In this work the results of the P219 experimental campaign are presented and more details are given for the shots on graphite specimens. The tests performed at the PHELIX laser facility provided a large amount of data which will be of paramount importance to benchmark and validate the current numerical models concerning laser-matter interaction and the resultant behavior of the material both in terms of shockwave propagation and spall failure for innovative materials with BIDs applications.

2.2. Petawatt high-energy laser for heavy ion experiments (PHELIX) facility

The present work provides an overview of the P219 experimental campaign conducted at the Petawatt HighEnergy Laser for Heavy Ion Experiments (PHELIX) at the GSI in Darmstadt. The laser produced square temporal pulses of 1.5 ns at a wavelength of 527 nm (2nd harmonic), delivering energies in the range of 40–70 J, with a focal spot obtained by a random phase plate of 1 mm diameter, resulting in a laser intensity in the range of 3.4–5.9 TW/cm^2. The laser energies are measured for each shot by a calorimeter from a pick-off mirror in the laser chain, and the data coming from the calorimeter have been cross-calibrated with the laser energies delivered inside the target chamber, i.e. the laser intensities provided are depurated by the energy loss in the phase plates. Nonetheless, one fifth of the energy transmitted after the phase plates is lost in diffraction of order higher than 1st, hence 80 % of the energy goes into the focal spot. The intensity of all the shots were corrected accordingly.

Targets were irradiated under vacuum, and a mechanized stage allowed to move from one irradiated specimen to a pristine one.

The spatial distribution of the PHELIX laser beam has been described in two studies: measuring the X-ray pinhole picture of the hot zone in the focal region [19] or the horizontal intensity profile at best focus [20]. The outcomes are shown in Fig. 1. Based on those descriptions, the simplified spatial profile is proposed to model the laser intensity distribution. The laser pulse temporal profile can be considered flat top in time with a plateau duration of 1.5 ns and fall times of 0.1 ns [21]. Knowing the deposited energy, the spatial and temporal profiles the laser intensity is calculated for each shot and shown in Table 2. Under these irradiation conditions the ablation pressure applied on the front surface of the sample can be estimated by semi-empirical scaling laws found in the literature [22] or via hydrodynamics simulation of the laser-matter interaction [23].

2.3. Targets

The targets were 10-mm-diameter discs with thicknesses ranging from 0.75 to 3.5 mm. The thickness of the specimens has been evaluated by means of hydrodynamic simulations with the aim of obtaining different levels of damage [23]. During the tests, different materials were tested, as detailed in the following paragraphs.

2.3.1. Materials

The first calibration shots were taken at well-known materials such as copper and aluminium. After these tests, 46 shots were fired at specimens made of different materials of interest for BIDs.

The isotropic polycrystalline graphite SIGRAFINE® R4550 by SGL Carbon SE (Germany) was among the tested specimens, since it is currently used for the Target Collimator Dump Injection (TCDI) collimators of the SPS-to-LHC transfer lines [24] and its behavior with copper coating will be investigated during Long-Shutdown 3 (LS3) at LHC [25]. Furthermore, hypervelocity impact and laser shock experimental characterization of a graphite similar to R4550 has already been made [26–28]. Density and properties can be varying depending on grade and commercial products, nevertheless isotropic graphite is commonly used in industry and in high energy domains of application. R4550 characterization under various impact loading is available [10], and a reference study based on laser-driven shocks has been performed at the LULI 2000 laser facility on a similar material [26–28].

In addition, the CFC FS140® produced by Tatsuno (Japan) was irradiated in this test. This material was chosen because it is similar to the grade used in the primary and secondary LHC collimators.

Several shots were dedicated to a novel composite material named Molybdenum carbide – Graphite (MoGr), which was tested under laser-shock impact for the first time.

The research on MoGr was started with the aim of increasing the

Table 1
Relevant properties of the materials used in the experiment. The longitudinal elastic wave velocity is calculated for uniaxial stress assumption based on $C_{uniaxial} \approx \sqrt{E/\rho}$, where E is the Young modulus and ρ is the material density.

Material	Grade	Density [g/cm^3]	Orientation	Young Modulus [GPa]	$C_{uniaxial}$ [m/s]
Graphite	R4550	1,9	Iso.	11,5	2460
MoGr	Nb8304Ng	2,55	IP	60	4851
			TP	4	1252
MoGr	Denser grade	2,7	IP	83	5544
			TP	9	1853
CrGr	as tested in [32]	2,15	IP	38	3752
			TP	2,5	1078
CFC	FS140	1,7	IP	75	5906
			TP	3	1328
CuCD	B1000	5,3	Iso.	194	6050
CuGr	–	5,26	Iso.	80	3900

electrical conductivity of primary and secondary collimators made of CFC, while maintaining robustness to beam impact. MoGr is produced by Spark Plasma Sintering at a temperature of 2600 °C which is above the melting point of molybdenum carbide. At this high temperature the molybdenum reacts with carbon, forming carbides with a surprisingly good electrical conductivity. The development of MoGr required an extensive process optimisation of powder composition and type, as well as of temperature and pressure of the sintering [29]. In order to assess the compatibility to particle accelerator requirements the MoGr Ultra-High Vacuum (UHV) behavior was described [30]. Moreover, MoGr was submitted both to an ions irradiation campaign at the M-Branch of the UNILAC accelerator at GSI [31] and a proton irradiation campaign at CERN HiRadMat facility [16]. Collimators made of graphite-matrix composites reinforced with Molybdenum carbides (MoGr) have been installed during (Long Shutdown 2) LS2 replacing the Carbon-carbon composite CFC collimators. Such collimators are under operation, for the first time at CERN during LHC Physics Run 3. In the detail, the chosen grade of MoGr is the Nb8304Ng produced by Nanoker (Spain), which is installed in the updated HL-LHC collimator absorbers. As a comparison, another denser grade of MoGr was also tested, the grade NB2507Ng produced by Nanoker (Spain). In the effort of developing a cheaper and low-environmental impact material, an alternative material to MoGr named Chromium Carbide – Graphite (CrGr) was tested. Besides the properties related to the application in the BIDs, one of the objectives of the material development is to reduce material and production cost. Keeping the advantage of the carbide graphite composite, the replacement of the molybdenum as catalysis by chromium has been considered and Chromium carbide – Graphite (CrGr) was developed, characterised [29] and tested under proton radiation [32].

Table 2
Summary of the shots performed. The coatings between brackets are non-functional coatings.

Material	Thickness [μm]	Coating	Shot Id.	Laser Intensity [TW/cm2]	Debris Velocity HSC [m/s]	Max. Surface Velocity PDV [m/s]	Time max. vel. PDV [μs]	Shockwave travel time Streak Camera [µs]	Average wave speed PDV [m/s]	Average wave speed Streak Camera [m/s]
Copper	200	–	2	2,6	0	1063	0,184		1085	
Aluminium	500	–	3	4,5	0	2241	0,164		3056	
Graphite	750	(Ag)	1	3,4	148	222	0,696		1078	
		(Marker)	41	3,8	177	243	0,465	0,283	1613	2648
	1000	(Marker)	35	4,4	150	180	0,604	0,317	1656	3151
		Cu	27	3,8	22	71	0,995		1507	
	1500	(Marker)	34	3,9	16	69	0,926	1,006	1620	1491
	2000	(Marker)	33	3,8	16	64	1,226	1,113	1632	1796
MoGr IP	750	(Ag)	4	3,1	172					
		(Ag)	37	4,1	172	213	0,327	0,376	2294	1995
	1000	(Ag)	28	3,8	91	167	0,465	0,386	2149	2592
	1500	Mo	6	3,4	44					
		Cu	8	3,8	56	110	0,696	0,654	2156	2293
		Cu + Tape	9	3,8		115	0,880	0,703	1704	2133
		(Ag)	10	3,7	78	110	0,880	0,625	1704	2400
	2000	(Ag)	29	3,8	57	91	1,111	1,025	1801	1950
	2750	(Marker)	13	4,0		51	1,641	1,592	1676	1728
	3500	(Marker)	15	4,5		33	2,470		1417	
MoGr TP	750	(Ag)	5	3,4						
		(Marker)	7	4,1		210	0,258	0,166	2906	4518
		(Ag)	39	3,8	132	165	0,327	0,278	2292	2695
	1000	(Ag)	38	4,6	98	155	0,465	0,386	2151	2592
	1500	(Ag)	11	3,6	19	58	0,811	0,703	1849	2133
	2000	(Ag)	17	3,9		40	1,203	0,938	1663	2133
	2750	(Marker)	14	3,9		19	0,100		27630	
	3500	(Marker)	16	3,8						
MoGr Denser IP	1500	(Ag)	21	3,3	51	112	0,488	0,439	3071	3413
	2250	(Marker)	25	4,2	0	71	1,018	0,928	2209	2425
MoGr Denser TP	1500	(Ag)	22	3,2	46	35	0,673	1,221	2229	1229
CFC IP	1500	(Ag)	20	3,8	76	100	1,595	1,074	941	1396
	2250	(Marker)	36	4,2	0	59	1,963		1146	
CFC TP	1500	(Ag)	24	3,7	59	65	1,318		1138	
3D CFC IP	1500	(Ag)	44	3,9	0	36	0,748	0,420	2007	3572
3D CFC TP	1580	(Marker)	47	3,8	0	46	0,373	0,195	4233	8090
CrGr IP	1500	(Ag)	12	3,5	108	115	1,065	0,928	1409	1617
	2250	(Marker)	23	3,7	0	72	1,433	1,416	1570	1589
CrGr TP	1500	(Ag)	19	3,4	46	43	1,249		1201	
CuCD	750	(Marker)	26	4,2	134	130	0,258		2906	
	1000	(Marker)	18	3,5	58	62	0,420		2381	
CuGr	750	(Ag)	45	3,9	140	106	0,281	0,225	2668	3339
	1530	(Marker)	46	3,7		63	1,318	0,146	1161	10445

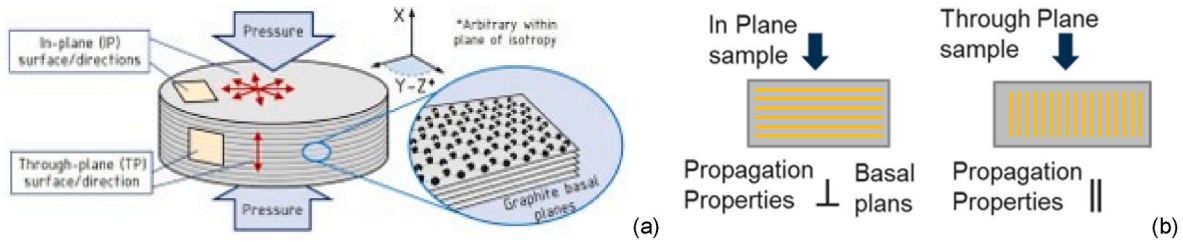

Fig. 2. Schematic description of the basal plan orientation (a) with respect to the pressure applied during manufacturing processes [29] and (b) with respect to the pressure applied on the specimen during the experiment.

Another composite of interest for BIDs is CopperDiamond (CuCD). This composite is produced by SolidPhase sintering at a temperature slightly lower than the melting temperature of copper. The composition of the powder is 60 % diamond, 39 % copper and 1 % boron. The diamond particles are dispersed in the copper matrix and have various sizes in order to enhance the material compaction. The boron is added to overcome the low chemical affinity between diamond and copper. Even though the CuCD also has very good thermal and electrical conductivity, it is extremely difficult and expensive to produce and to machine. This composite has shown superior robustness to beam impact compared to other alloys (W or Mo-based) envisaged for tertiary collimators. The online and post-mortem results of experimental campaigns at HiRadMat concerning materials for BIDs have been presented in various papers [32–36]. Indeed, extensive simulation work has been done to benchmark the results gathered in the experimental campaigns [36–38]. As a potential alternative to CuCD, also Copper – Graphite (CuGr) was tested.

2.3.2. Orthotropic directions

Carbide-graphite composites, as well as CFC composites, are mainly composed of oriented graphite, therefore they exhibit an orthotropic behavior. The dynamic behavior of those anisotropic materials has been investigated by measuring the propagation of the pressure waves in both orthotropic directions after the application of a pressure field. Table 1 shows the properties of the materials in the two directions. The naming convention used in this work is presented in the following and in Fig. 2. The orientation of the basal planes in the sample depends on the uniaxial pressure applied during the manufacturing. An anisotropic sample is named in-plane (IP) if the specimen was cut in the direction of the graphite basal plane. In that case, impact loading pressure generated by laser driven shock is applied perpendicularly to the graphite basal planes. On the contrary, a sample is named through-plane (TP), if the specimen was cut perpendicularly to the direction of the graphite basal plane, and so the pressure loading and the wave propagation are parallel to the basal planes of the material.

The preferred orientation of graphite basal planes is defined with respect to the applied uniaxial pressure during manufacturing. The naming convention for the material directions used in this study is referred to previous works [29].

2.3.3. Coatings

Since thin-film are deposited on the collimator absorbers of the LHC to enhance electrical conductivity, their adhesion was also investigated during this test campaign. Taking advantage of irradiation conditions close to those of a LAser Shock Adhesion Test (LASAT) used to assess the bonding strength of coating and adhesives, 6-μm-thick molybdenum coatings and 3-μm-thick copper coatings were applied on the back face of some of the targets. However, due to their low reflectivity, the presence of this coating was detrimental to the quality of the signal from online diagnostics (PDV and Streak camera), and for this reason this configuration was limited to a few shots. In addition to that functional coating, a coating aiming at enhancing the back surface reflectivity was applied on the sample as further explained in following sections.

Table 1 gathers some of the main properties of the materials used for this experiment under laser pulses.

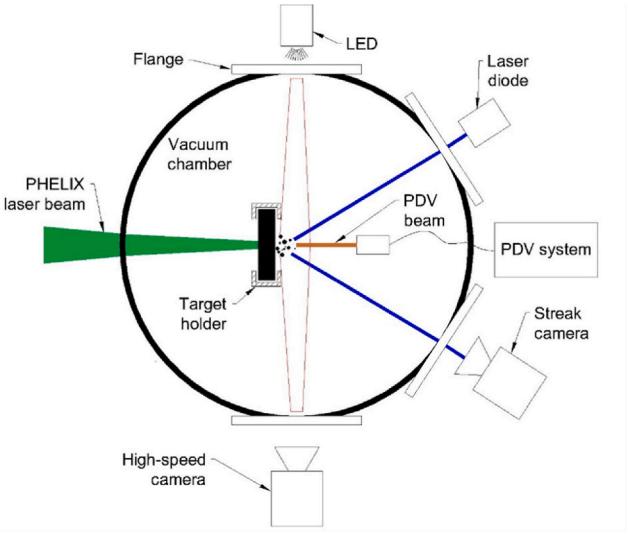

Fig. 3. Schematic of the online diagnostics used during the experimental campaign.

2.3.4. Diagnostics

During the P219 experimental campaign, both, on-line and post-mortem diagnostics have been used. In Fig. 3 a schematic of the on-line diagnostics used during the experimental campaign is reported. Photonic doppler laser velocimetry (PDV) was installed pointing at the back surface of the specimen to measure the back surface velocity when the shockwave broke out. Nevertheless, the temporal resolution was limited to 55 ns. Facing the challenges due to the low reflectivity of the target, several methods were used to enhance the return signal in the 1.5-mm-diameter PDV probe: surface polishing, 1-µm-thick silver flash coating, or application of reflecting silver colour ink. A fine adjustment of the alignment of the incident and reflected probe beam was also required. The VISAR installed in PHELIX facility [21] relies on streak camera allowing a measurement window of 30 ns. Based on preliminary simulation, it was shown that this measurement window was incompatible with the time scale of the shock-wave arrival on the back surface. The streak camera was nevertheless used to point directly at the back surface without interferometry system. Streak images, recorded with a 16 bits CDD with 1344 × 1024 pixels could define the time at which the shock broke out of the back surface of the specimen with a temporal resolution in the range of 65–120 ns, depending on the choice of the sweep window. High speed systems based on shadowgraphy was implemented for transverse imaging of the debris ejection. With photo diode enlightenment, the camera took 26.6-μm-pixel-size pictures of the cloud of debris, every 1.7–5.4 µs. Opening and closing time of the shutter were recorded on oscilloscope to determine the exact time of the capture, while the exposure time was fixed at 369 ns. Ejected debris were collected on a transparent PMMA plate placed at 12 mm from the back

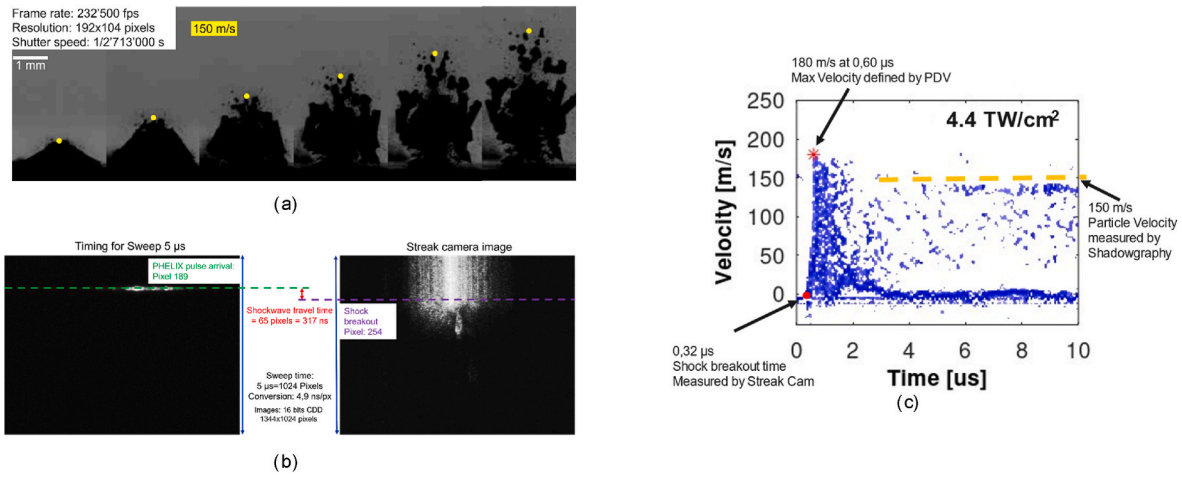

Fig. 4. Experimental data from the shot on 1000 µm graphite target: (a) shadowgraphy from high-speed camera (b) acquisition from streak camera, (c) PDV data with comparison between data from all the diagnostics.

surface. The shape and size of debris will be analysed by scanning electron microscopy. Ultimately, post-mortem microscopy and tomography of the specimens submitted to laser impact will be deployed to measure the crater on the front surface, the spallation depth on the back surface and to localize the subsurface cracks.

2.3.5. *Post-mortem analysis*

Post-mortem analyses were carried out using two advanced imaging systems: the Keyence digital microscope VHX-7000 and the Veeco 3D Optical 3D profiling and roughness system. The Keyence digital microscope was used to first obtain high-resolution images of the damage induced on the specimens, allowing for detailed observation of the craters on the front and back surfaces. An "in-depth" 2D profile analysis of the craters was then performed to evaluate the variations in shape and depth of the laser-induced damage on both the front and back side of each specimen. For this purpose, the roughness and profiling capabilities of the Keyence microscope were employed. The same type of analysis was done using the Veeco 3D Optical 3D profiling and roughness system, which is known for its highly accurate surface roughness measurement functions, with a maximum height range of 2 mm in Vertical Scanning Interferometry (VSI) mode and an accuracy of $\pm$ 1.50 nm.

The findings from the Keyence digital microscope and Veeco system were consistent, both showing similar variations in the shape and depth of the laser-induced craters. This comparison of results between the two systems provides valuable cross-validation and confidence in the conclusions reached through the post-mortem analysis.

3. Experimental results

3.1. *Pulse list and results overview*

The pulse list given in Table 2 summarizes for each shot the characteristics of the target (material, coating and thickness), the laser intensity, the average velocity of the debris measured by the High-Speed Camera (HSC), the maximum back surface velocity and the average breakthrough time measured by the PDV and by the streak camera. The laser pulse duration of 1.5 ns and spatial distribution are considered constant. From the results it is possible to highlight the complementarity of the diagnostics. The PDV was able to determine the peak velocity of the back surface of the material with adequate precision, while the streak camera measured the time that the shock-wave needed to travel through the specimen. Indeed, the high-speed camera was the only diagnostic to record the failure mechanism of the various specimens and it also gave the possibility to evaluate the average speed of the debris flying off the material, which is fundamental to estimate the spall stress. As already said, the low reflectivity of the surfaces played an important role for the data acquisition of both PDV and streak camera systems, hence causing the loss of signal during some shots.

The waves speeds determined by the PDV and Streak Camera timings and the specimens' thicknesses could be compared to the longitudinal elastic wave speeds reported in Table 1. It should be recalled that the elastic wave velocities were recorded with a uniaxial stress assumption, hence their validity becomes lower as the thickness of the specimen increases. As a matter of fact when the specimen thickness becomes equal or greater than the focal spot of the laser of 1 mm, the uniaxial approximation looses validity since the shockwave tends to become spherical, thus providing bidimensional features.

Furthermore, the disturbance travel times acquired by the PDV and the Streak Camera are significantly different from each other. The present effect might be explained by the fact that the Streak Camera records the first movement of the back surface, hence capturing the elastic precursor, while the PDV indicates the maximum speed, hence the arrival of the plastic wave.

In view of the conclusion drawn, it becomes more clear why for example the average wave speed determined by the Streak Camera for the shot 41 is close to the uniaxial elastic wave speed declared in Table 1, while the other wave speeds seem inconsistent with the data in Table 1.

3.2. *Example of data analysis - shot on 1000-µm-thick graphite target*

The shot on the 1000 µm graphite target is taken as an example to describe the data analysis which follows the data acquisition from the diagnostics. From the frames acquired with the high-speed camera the debris detaching from the back surface can be tracked and their average velocity can be easily estimated by knowing the distance covered between two frames and the frame rate of the camera, as shown in Fig. 4. As previously mentioned, the streak camera was used to define the time at which the shockwave arrived at the back surface of the specimen, which can be used to determine the average shock-wave speed inside the material. Indeed, the shockwave speeds evaluated in Table 2 can be only qualitatively compared to the shockwave speeds from Table 1 since in the laser experimental conditions the produced shockwaves are not perfectly planar shockwaves.

The streak camera image in Fig. 4 should be read from the top to the bottom because this is the timeline of the shot. When the horizontal pattern of the image changes it means that the streak camera system has detected a movement of the back surface of the specimen, signifying that the shockwave has arrived. Since the PHELIX laser shock pulse arrival on the front surface is known thanks to the synchronisation system of the facility, the shockwave travel time can be evaluated as the difference

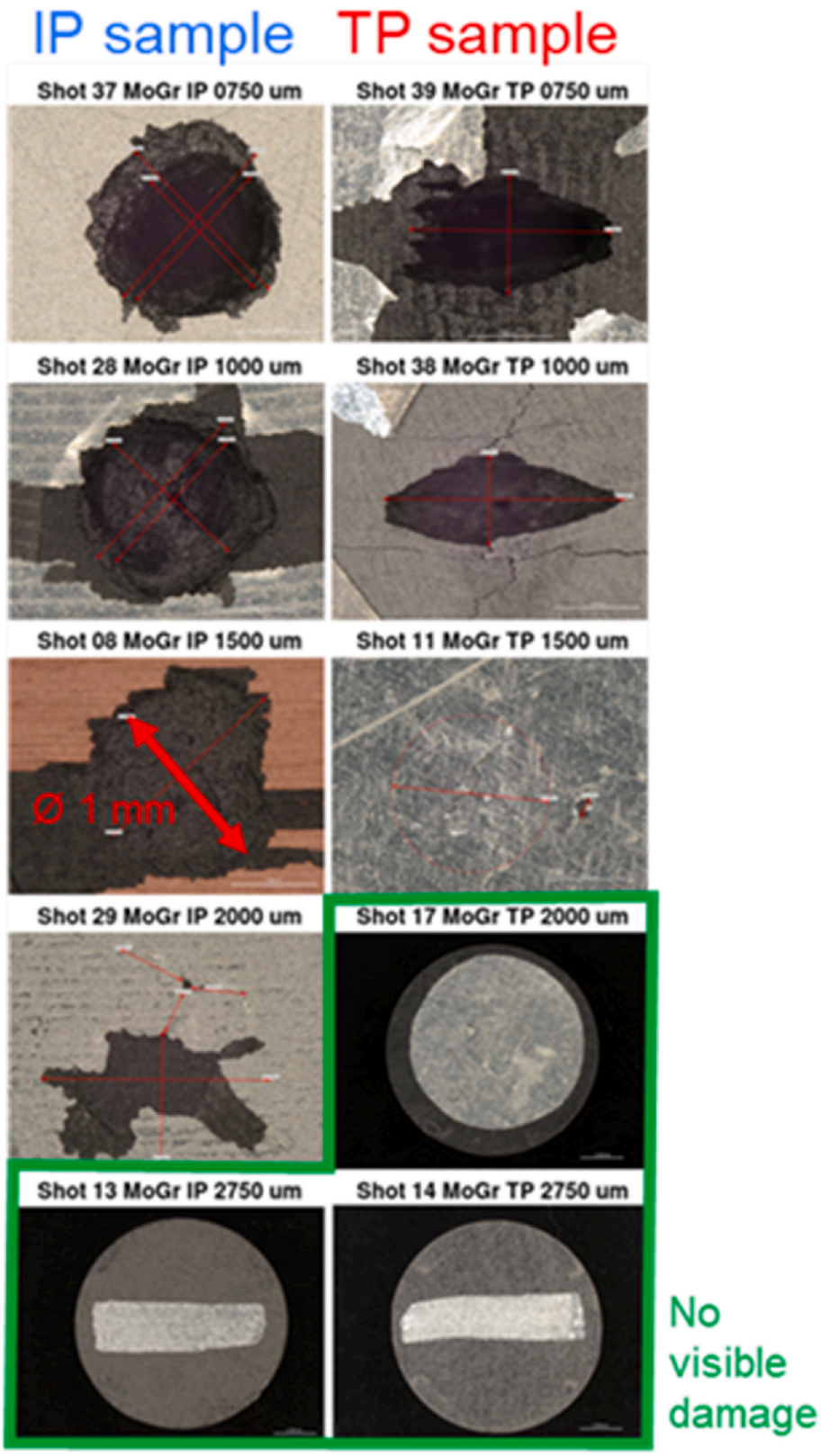

Fig. 5. Microscopies of the post mortem MoGr IP and TP specimens back surfaces.

between the time of shock breakout and the time of pulse arrival. Finally, the PDV system was able to determine the maximum speed of the shockwave breaking out of the back surface and to confirm the speed of the debris evaluated by the high-speed camera and the time of shockwave breakout measured by the streak camera, as shown in Fig. 4.

4. Discussion

In addition to the overview of the results, two study cases are given in the following: one based on the complementarity of the diagnostics and the other aiming at comparing data obtained during experimental

Table 3
Comparison of quasi-static bending strength measured in former works and spall strength obtained by acoustic assumption, derived from PHELIX "P219" experiment measurements.

Material	Grade	Orientation	Quasi-Static bending strength [MPa]	Spall strength [MPa]
Graphite	R4550	Iso.	61	125
MoGr	Nb8304Ng	IP	10	76
		TP	80	267
MoGr	Denser grade	IP	–	309
		TP	–	–
CrGr	as tested in [32]	IP	5	8
		TP	26	–
CFC	FS140	IP	10	21
		TP	160	28
CuCD	B1000	Iso.	300	35
CuGr	–	Iso.	50	–

campaigns performed on similar materials.

4.1. Orthotropic materials, comparison of damage observed depending on the direction of stress

Fig. 5 presents the general aspect of the target back surface for MoGr specimen, taking into account the direction of stress and the thickness of the target. When the target thickness increases, the damages observed on the back surface are reduced. Qualitative comparison of the back surface damages allows the comparison of the ability to withstand the dynamic stress. When comparing the damages on IP and TP MoGr targets, it appears that the IP direction is weaker than the TP direction as it was observed during quasi-static bending tests (Table 3). An evaluation of the spall strength in both cases is proposed in the following.

Fig. 6 shows the crater profile observed on the back surface of IP MoGr and TP MoGr targets. Both the depth and the volume of the craters observed under similar irradiation conditions are more remarkable for TP MoGr specimen.

The pullback velocity is evaluated as the difference between the maximum of the free surface measured by the PDV and the debris velocity measured by the HSC. All the data acquired through the present work are shown in Table 2. The back surface velocities acquired for MoGr targets are plotted in Fig. 7 taking into account the direction of the basal planes depending on the shock propagation, as a function of the target thickness.

The spall strength is evaluated based on the pull back velocity under the acoustic assumption [26]:

$$\sigma_{sp} = \frac{1}{2}\rho_0 C_0 \Delta u_{pb} \tag{1}$$

where C_0 is the bulk sound velocity in $[m/s]$, ρ_0 is the density in $[kg/m^3]$ and Δu_{pb} is the pullback velocity obtained experimentally. The material properties used for each material are taken from Table 1. The averaged values of spall strength, resulting from the current post-experimental study are given in Table 3 and compared to the quasi-static bending strength measured in former works [32]. It is worth noting that given the porosity of the materials used in the study, the acoustic approximation must be considered with caution [26].

In further works, assisted by numerical simulation, such diagnostics

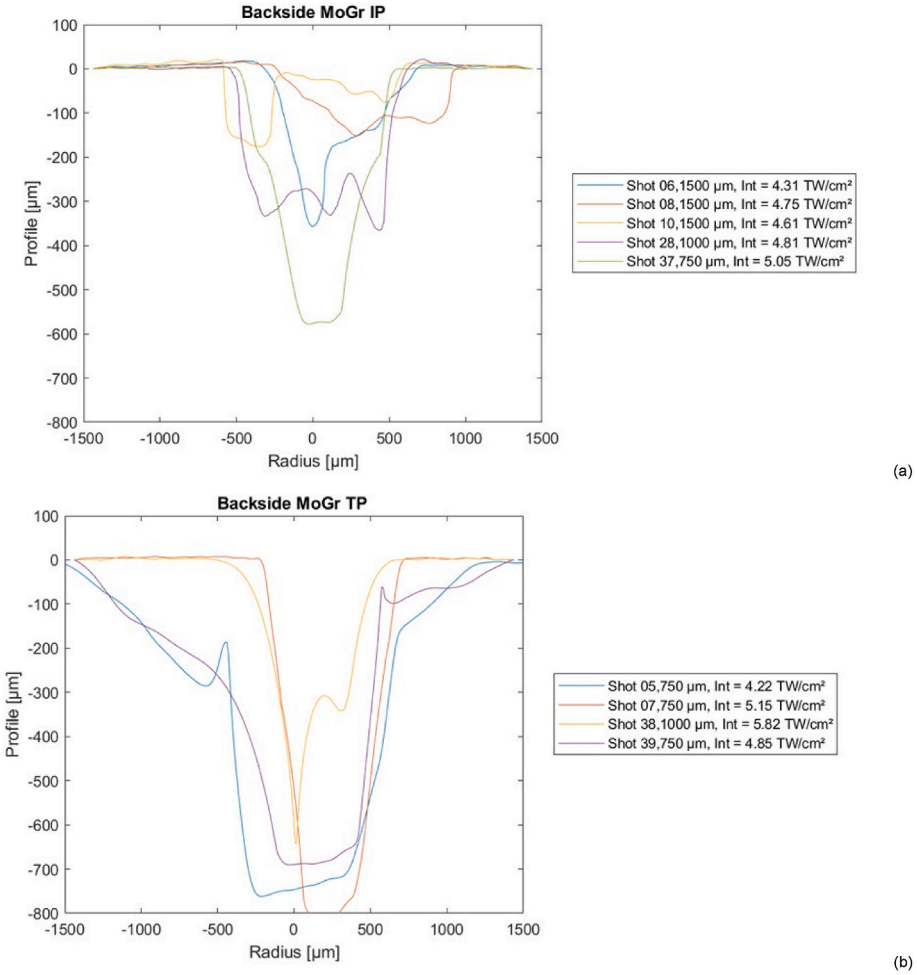

Fig. 6. Profilometries of the backsurfaces of postmortem MoGr (a) IP samples and (b) TP samples.

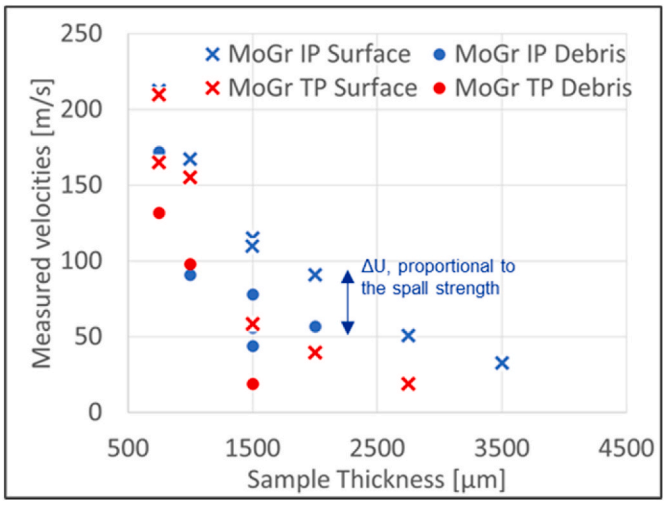

Fig. 7. Experimental peak sample surface speed and detached debris speed, for IP and TP MoGr samples, as a function of the initial sample thickness.

should both allow to evaluate the loading conditions into the targets and get an insight into the resulting damage phenomena in materials under high strainrate loading.

4.2. Graphite comparison with studies from literature

Fig. 8 presents the results of the PDV measurements performed on graphite targets. The conditions of irradiation during each of these cases can be found in Table 2.

Besides application in particle accelerator, graphite is a material commonly used in high energy industrial applications, such as nuclear reactors. Similar graphite materials have been submitted to laser shocks, and the results are reported in the literature. Laser-driven shocks with nano and picosecond laser irradiation at Kamerton-T and at PHELIX facility respectively, on different grades of Graphite (Graphite MF-307 and Polycrystalline Graphite PG-5) [18,19]. Back surface velocity was not monitored during the aforementioned experiments, but damages and material transformation on the front and back surface were characterised by Optical microscopy and Raman spectroscopy, and the spalled regions thicknesses were measured. A reference study based on laser-driven shocks has been performed at the LULI 2000 laser facility, on a similar material, named EDM3, which is a porous isotropic and homogeneous graphite from POCO Company [26–28]. The material had also been characterised at smaller strain rate under hyper-velocity impacts obtained by projectiles launched by MICA, a two-stage light-gas gun located at CEA CESTA [39,40]. A simulation benchmark of the laser shocks experiment on porous graphite EDM3 was performed in a previous work [23]. In this work, it is proposed to compare the maximum back surface velocities extracted during the two experimental campaigns. It is worth noting that even though the two materials are similar, they are not strictly identical since the density is different. Indeed, a higher density means lower dissipation of the disturbance. Moreover, the characteristics of the laser pulse provided by the two facilities are also slightly different from the point of view of the spatial profile and the pulse duration. In particular, the energies delivered by the LULI laser are higher than the GSI laser. For these reasons the maximum back surface velocities can be compared only if they are normalized by the maximum laser intensity, the pulse duration and density of the tested graphite, as shown in Fig. 9. As it seems from the comparison of the normalized maximum speed the data acquired during the two experimental campaigns are relatable. However, the normalization shown in Fig. 9 is able to only give a rough estimation of the analogies between the shots taken in different conditions. As a matter of fact, simulations need to be performed to completely understand the phenomena involved.

5. Conclusion and future work

In the present work the motivations and the results of the P219 experimental campaign were presented. The laser-shock tests performed at the PHELIX laser facility of the GSI research center in Darmstadt (Germany) provided a large amount of data. Globally, 48 samples were tested under high intensity laser, all the specimens were made of

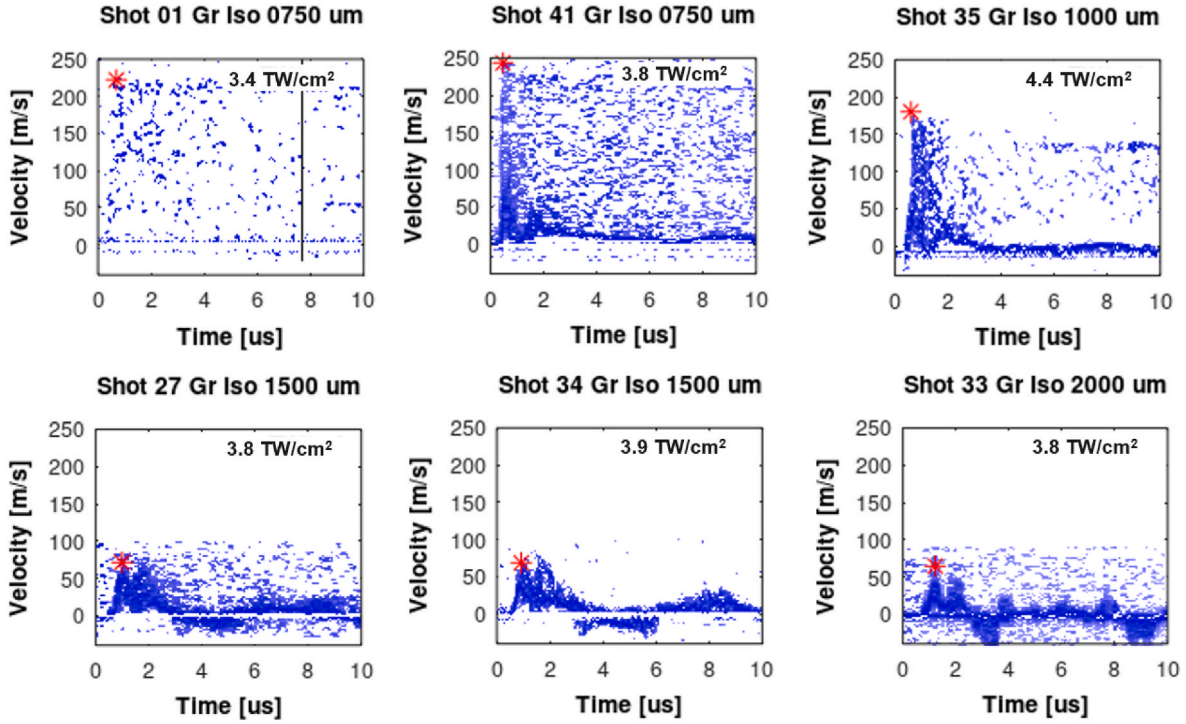

Fig. 8. PDV measurement performed during shots on graphite specimens. The back surface velocity is recorded for specimens of various thicknesses.

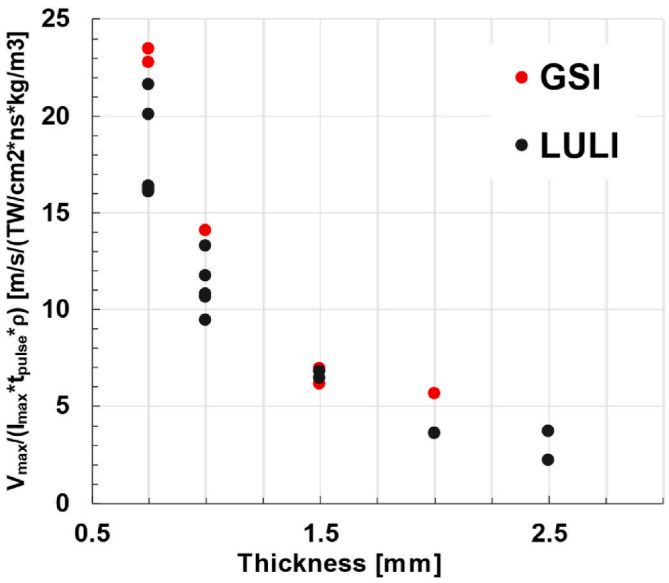

Fig. 9. Comparison between GSI and LULI shots of the maximum speed of the back surface determined by the PDV (V_{max}) normalized by the maximum laser intensity of the shot (I_{max}), the duration of the pulse (t_{pulse}) and the density of the specimen (ρ) in function of the thickness of the specimen.

materials relevant for particle accelerators BIDs application. The isotropic graphite R4550 was taken as reference material, since it is well-known. However, cutting-edge materials, namely MoGr, CuCD, CuGr and CrGr were irradiated as well.

During the shots, the phenomena happening on the back surface of the specimen were recorded by means of several diagnostics, such as a PDV laser velocimeter, a streak camera and a high-speed camera. Indeed, post-mortem analysis by means of scanning electron microscopy and tomography were performed.

The combination of online and post-mortem diagnostics provided fundamental information on the damage observed on different materials submitted to laser-shocks and will permit to quantitatively compare the different materials. Surely, the acquired experimental data will allow to benchmark and enhance the actual simulation procedure in terms of materials constitutive models for laser-matter interaction, shockwave propagation and spall strength for a variety of innovative materials specifically developed for beam intercepting devices of particle accelerators.

CRediT authorship contribution statement

C. Accettura: Writing – review & editing, Writing – original draft, Supervision, Project administration, Methodology, Investigation, Formal analysis, Data curation. **L. Baudin:** Writing – review & editing, Writing – original draft, Software, Investigation, Formal analysis, Data curation. **A. Bertarelli:** Writing – review & editing, Supervision, Investigation, Formal analysis, Conceptualization. **C. Brabetz:** Software, Resources, Methodology. **F. Carra:** Writing – review & editing, Resources, Project administration, Investigation, Data curation. **A.S. Martynenko:** Investigation. **A. Morena:** Writing – review & editing, Writing – original draft, Software, Investigation, Data curation. **A. Moros:** Writing – review & editing, Data curation. **L. Peroni:** Writing – review & editing, Supervision, Resources, Project administration. **M. Scapin:** Writing – review & editing, Resources, Project administration. **P. Neumayer:** Investigation. **M. Tomut:** Supervision, Project administration. **L. Wegert:** Investigation.

Declaration of competing interest

The authors declare that they have no known competing financial interests or personal relationships that could have appeared to influence the work reported in this paper.

Acknowledgments

The authors wish to thank Luca Gentini for the sample holder design and Isadora Cavassani and Didier Glaude for the microscopy analysis. A particular thank goes to BrevettiBizz and Nanoker for supplying the material for the irradiation campaign and IDIL Optic Fiber Mehdy Giroux who provided and operated the PDV system. We want also to thank GSI for the help with the transport and the set-up of the measurements. The results presented here are based on the experiment PHELIX Z6, at the GSI Helmholtzzentrum fuer Schwerionenforschung, Darmstadt (Germany) in the frame of FAIR Phase-0. The research leading to these results has received funding from the European Union's Horizon 2020 Research and Innovation program under Grant Agreement n. 73087.

Data availability

Data will be made available on request.

References

[1] O. Bruning, P. Collier, P. Lebrun, S. Myers, R. Ostojic, J. Poole, LHC design report v.2, CERN Yellow Reports: Monographs, 2004.
[2] O. Bruning, L. Rossi, The High Luminosity Large Hadron Collider, in: Vol. 24 of Advanced Series on Directions in High Energy Physics, 10, World Scientific, 2015.
[3] G. Apollinari, I. Bejar Alonso, O. Bruning, P. Fessia, M. Lamont, L. Rossi, L. Tavian, High-luminosity large Hadron Collider (HL-LHC), CERN Yellow Reports: Monographs, cern yellow ed., Geneva, Switzerland, 2017. Technical Design Report V. 0.1.
[4] Abada, et al., FCC-hh: the Hadron Collider, Eur. Phys. J. Spec. Top. 228 (7 2019) 755–1107.
[5] R. Bruce, A. Abramov, A. Bertarelli, M.I. Besana, F. Carra, F. Cerutti, A. Faus-Golfe, M. Fiascaris, G. Gobbi, A. Krainer, A. Lechner, A. Mereghetti, D. Mirarchi, J. Molson, M. Pasquali, S. Redaelli, D. Schulte, M. Serluca, E. Skordis, M. Varasteh, Collimation system studies for the FCC-hh, J. Phys. Conf. Ser. 1350 (2019) 12009–12011.
[6] E. Quaranta, Investigation of Collimator Materials for High Luminosity Large Hadron Collider, POLITECNICO DI MILANO, 2017. PhD thesis.
[7] A. Bertarelli, A. Dallocchio, M. Garlasche, L. Gentini, P. Gradassi, M. Guinchard, S. Redaelli, A. Rossi, O. Sacristan de Frutos, F. Carra, E. Quaranta, Novel materials for collimators at LHC and its upgrades, in: Proceedings of the 54th ICFA Advanced Beam Dynamics Workshop on High-Intensity, High Brightness and High Power Hadron Beams, HB 2014, 2015, pp. 438–442, no. 312453, (EastLansing).
[8] A. Bertarelli, Beam-induced damage mechanisms and their calculation, in: Proceedings of Joint International Accelerator School: Beam Loss and Accelerator Protection, 2, 2014, pp. 159–227.
[9] G. Gobbi, A. Bertarelli, F. Carra, J. Guardia-Valenzuela, S. Redaelli, Novel LHC collimator materials: high energy Hadron beam impact tests and non-destructive post-irradiation examination, Mech. Adv. Mater. Struct. 27 (17) (2020) 1518–1530.
[10] L. Peroni, M. Scapin, F. Carra, N. Mariani, Investigation of dynamic fracture behavior of graphite, Key Eng. Mater. 569–570 (7 2013) 103–110.
[11] M. Scapin, L. Peroni, M. Peroni, Parameters identification in strain-rate and thermal sensitive visco-plastic material model for an alumina dispersion strengthened copper, Int. J. Impact Eng. 40–41 (feb 2012) 58–67.
[12] M. Scapin, Mechanical characterization and modeling of the heavy tungsten alloy IT180, Int. J. Refract. Metals Hard Mater. 50 (May 2015) 258–268.
[13] M. Scapin, L. Peroni, F. Carra, Investigation and mechanical modelling of pure molybdenum at high strain-rate and temperature, J. Dyn. Behav. Mater. 2 (4) (2016) 460–475.
[14] M. Scapin, L. Peroni, C. Torregrosa, A. Perillo-Marcone, M. Calviani, L.G. Pereira, F. Leaux, M. Meyer, Experimental results and strength model identification of pure iridium, Int. J. Impact Eng. 106 (aug 2017) 191–201.
[15] M. Scapin, L. Peroni, C. Torregrosa, A. Perillo-Marcone, M. Calviani, Effect of strain-rate and temperature on mechanical response of pure tungsten, J. Dyn. Behav. Mater. 5 (3) (2019) 296–308.
[16] F.J. Harden, A. Bouvard, N. Charitonidis, Y. Kadi, HiRadMat: a facility beyond the realms of materials testing, J. Phys. Conf. Ser. 1350 (2019), 012162, 11.
[17] A. Bertarelli, V. Boccone, F. Carra, F. Cerutti, A. Dallocchio, N. Mariani, L. Peroni, M. Scapin, Limits for beam induced damage: reckless or too cautious?, in: Proceedings - Chamonix 2011 Workshop on LHC Performance, 2011, pp. 183–188.

[18] I.K. Krasyuk, A.Y. Semenov, I.A. Stuchebryukhov, R.S. Belikov, K.V. Khishchenko, O.N. Rosmej, T. Rienecker, A. Schoenlein, M. Tomut, Investigation of the spall strength of graphite using nano- and picosecond laser pulses, J. Phys. Conf. Ser. 653 (2015) 12002–12011.
[19] R.S. Belikov, I.K. Krasyuk, T. Rinecker, A.Y. Semenov, O.N. Rosmej, I. A. Stuchebryukhov, M. Tomut, K.V. Khishchenko, A. Schoenlein, Negative pressure and spallation in graphite targets under nano- and picosecond laser irradiation, Quant. Electron. 45 (2015) 421–425.
[20] W. Cayzac, Analysis of the new 1 mm PHELIX random phase plate (RPP) Vol. I, GSI Helmholtzzentrum fur Schwerionenforschung, Darmstadt, Germany, 2014, pp. 273–274, tech. rep.
[21] K. Jakubowska, D. Mancelli, R. Benocci, J. Trela, I. Errea, A.S. Martynenko, P. Neumayer, O. Rosmej, B. Borm, A. Molineri, C. Verona, D. Cannatà, A. Aliverdiev, H.E. Roman, D. Batani, Reflecting laser-driven shocks in diamond in the megabar pressure range, High Power Laser Sci. Eng. 9 (2021) e3.
[22] J. Lindl, Development of the indirect-drive approach to inertial confinement fusion and the target physics basis for ignition and gain, Phys. Plasmas 2 (1995) 3933–4024.
[23] A. Morena, L. Peroni, Numerical simulations of laser-induced shock experiments on graphite, Materials 14 (2021) 7079.
[24] F. Maciariello, O. Aberle, M. Butcher, M. Calviani, R. Folch, V. Kain, K. Karagiannis, I. Lamas Garcia, A. Lechner, F.-X. Nuiry, G. Steele, J. Uythoven, High Intensity Beam Test of Low Z Materials for the Upgrade of SPS-to-LHC Transfer Line Collimators and LHC Injection Absorbers, 2016, p. TUPMB052.
[25] C. Accettura, N. Biancacci, R. Bruce, F. Carra, N. Mounet, A. Kurtulus, F.-X. Nuiry, A. Perillo Marcone, S. Redaelli, Overview of Material Choices for hl-lhc Collimators, vol. 23, Proceeding IPAC, 2023.
[26] G. Seisson, G. Prudhomme, P.-A. Frugier, D. Hebert, E. Lescoute, A. Sollier, L. Videau, P. Mercier, M. Boustie, L. Berthe, Dynamic fragmentation of graphite under laser-driven shocks: identification of four damage regimes, Int. J. Impact Eng. 91 (5 2016) 68–79.
[27] G. Seisson, Etude experimentale et theorique de l' endommagement du graphite sous sollicitation dynamique – Application aux impacts hyperv'eloces, Ecolé Nationale Supérieure de Mécanique et d' Aérotechnique, 2014. PhD thesis.
[28] G. Prudhomme, Etude du nuage de particules éject'eeś sous choc : apports de la Vélocim'etrie Hét'erodyne, Ecole Nationale Supérieure d'Arts et Métiers, 2015. PhD thesis.
[29] J. Guardia Valenzuela, Optimisation Graphite-Matrix Composites for Collimators in the LHC Upgrade, University of Zaragoza, 2019. PhD thesis.
[30] C. Accettura, M. Beghi, A. Bertarelli, G. Bregliozzi, Carra, G. Cattenoz, J. Guardia-Valenzuela, S. Redaelli, M. Taborelli, Ultra-high vacuum characterization of molybdenum-carbide graphite for HL-LHC collimators, J. Phys. Conf. Ser. 1350 (2019), 012085, 11.
[31] C. Accettura, Investigation of Radiation Damage Effects in HL-LHC Collimator Materials, POLITECNICO DI MILANO, 2021. PhD thesis.
[32] J. GuardiaValenzuela, Review of Multimat-2 test (HRMT57), in: 148th LHC Collimation Upgrade Specification Meeting, 2022.
[33] M. Cauchi, O. Aberle, R.W. Assmann, A. Bertarelli, Carra, K. Cornelis, A. Dallocchio, D. Deboy, L. Lari, S. Redaelli, A. Rossi, B. Salvachua, P. Mollicone, N. Sammut, High energy beam impact tests on a LHC tertiary collimator at the CERN high-radiation to materials facility, Phys. Rev. Spec. Top. Accel. Beams 17 (2014), 021004, 2.
[34] A. Bertarelli, E. Berthome, V. Boccone, F. Carra, F. Cerutti, N. Charitonidis, C. Charrondiere, A. Dallocchio, P. Fernandez Carmona, P. Francon, L. Gentini, M. Guinchard, N. Mariani, A. Masi, S.D. Marques dos Santos, P. Moyret, L. Peroni, S. Redaelli, M. Scapin, An experiment to test advanced materials impacted by intense proton pulses at CERN HiRadMat facility, Nucl. Instrum. Methods Phys. Res. Sect. B Beam Interact. Mater. Atoms 308 (2013) 88–99.
[35] G. Gobbi, A. Bertarelli, F. Carra, J. Guardia-Valenzuela, S. Redaelli, Novel LHC collimator materials: high energy Hadron beam impact tests and nondestructive postirradiation examination, Mech. Adv. Mater. Struct. 27 (9 2020) 1518–1530.
[36] M. Pasquali, A. Bertarelli, C. Accettura, E. Berthome, L. Bianchi, P. Bolz, F. Carra, C. Fichera, M.I. Frankl, T. Furness, G. Gobbi, P. Grosclaude, J. GuardiaValenzuela, M. Guinchard, M.D. Jedrychowsky, F.J. Harden, A. Lechner, P. Mollicone, P. D. Pastuszak, M. Portelli, S. Redaelli, E. Rigutto, O.S. de Frutos, P. Simon, Dynamic response of advanced materials impacted by particle beams: the MultiMat experiment, J. Dyn. Behav. Mater. 5 (9 2019) 266–295.
[37] F. Carra, A. Bertarelli, G. Gobbi, J. Guardia-Valenzuela, M. Guinchard, F. Harden, M. Pasquali, S. Redaelli, E. Skordis, Mechanical robustness of HL-LHC collimator designs, J. Phys. Conf. Ser. 1350 (Melbourne) (2019), 012083, 11.
[38] E. Quaranta, A. Bertarelli, R. Bruce, F. Carra, Cerutti, A. Lechner, S. Redaelli, E. Skordis, andP. Gradassi, Modeling of beam-induced damage of the LHC tertiary collimators, Phys. Rev. Accel. Beams 20 (2017) 91002–91009.
[39] G. Seisson, D. Hébert, I. Bertron, J.-M. Chevalier, E. Lescoute, L. Videau, P. Combis, F. Guillet, M. Boustie, L. Berthe, Dynamic behavior of a porous brittle material: experiments and modeling, Procedia Eng. 58 (2013) 715–723.
[40] D. Hebert, G. Seisson, J.L. Rullier, I. Bertron, L. Hallo, J.M. Chevalier, C. Thessieux, F. Guillet, M. Boustie, L. Berthe, Hypervelocity impacts into porous graphite: experiments and simulations, Phil. Trans. R. Soc. A Math. Phys. Eng. Sci. 375 (2017) 20160171.